Chemical Science

ROYAL SOCIETY OF CHEMISTRY

EDGE ARTICLE

View Article Online
View Journal | View Issue

Cite this: *Chem. Sci.*, 2022, **13**, 7821

All publication charges for this article have been paid for by the Royal Society of Chemistry

Received 3rd May 2022
Accepted 7th June 2022

DOI: 10.1039/d2sc02478k

rsc.li/chemical-science

Carbazole-2-carbonitrile as an acceptor in deep-blue thermally activated delayed fluorescence emitters for narrowing charge-transfer emissions†

Chin-Yiu Chan,‡*[a] Yi-Ting Lee,‡[a] Masashi Mamada,[a] Kenichi Goushi,[a] Youichi Tsuchiya,[a] Hajime Nakanotani[ab] and Chihaya Adachi *[ab]

This work reports a new acceptor for constructing donor–acceptor type (D–A type) blue thermally activated delayed fluorescence (TADF) emitters with narrowed charge-transfer (CT) emissions. A new acceptor core, carbazole-2-carbonitrile (CCN), is formed by the fusion of carbazole and benzonitrile. Three D–A type TADF emitters based on the CCN acceptor, namely **3CzCCN**, **3MeCzCCN**, and **3PhCzCCN**, have been successfully synthesized and characterized. These emitters show deep-blue emissions from 439 to 457 nm with high photoluminescence quantum yields of up to 85% in degassed toluene solutions. Interestingly, all CCN-based deep-blue TADF emitters result in narrow CT emissions with full-width at half-maximums (FWHMs) of less than 50 nm in toluene solutions, which are pretty narrower compared with those of typical D–A type TADF emitters. Devices based on these emitters show high maximum external quantum efficiencies of up to 17.5%.

Introduction

The research and development of narrow-emission materials, realizing a high colour purity of their photoluminescence (PL) or electroluminescence (EL), has attracted significant attention in recent years. Particularly, ultra-high-definition display panels that will be the BT 2020 standard have to be manufactured using narrow-emission materials; however, the reports on narrow-emission materials are mainly dominated by conventional fluorescent molecules, resulting in internal quantum efficiency (IQE) being limited to only 25%.[1–3]

A thermally activated delayed fluorescence (TADF) molecule that possesses a small singlet–triplet energy gap (ΔE_{ST}) can achieve an IQE of 100% by thermally converting triplet excitons into singlet excitons.[4–7] Conventional donor–acceptor type (D–A type) TADF molecules are designed by introducing a twisted angle between donor and acceptor moieties, avoiding the significant overlap of the high occupied molecular orbital (HOMO) and lowest unoccupied molecular orbital (LUMO).[4,5] D–A type TADF molecules always possess strong charge-transfer characteristics that give rise to broadband emission with full-width at half-maximums (FWHMs) of 60 to 100 nm in the solution state.[5] In 2016, on the other hand, Hatakeyama and co-workers reported a new type of thermally activated delayed fluorescence molecule, namely a multi-resonance emitter (MRE), in which the multi-resonance effect of the boron and nitrogen atoms induces significant separation of the HOMO and LUMO on different atoms, minimizing the overlap of their bonding/antibonding characteristics.[8] MREs not only show TADF properties but also show narrowband emission that is as narrow as the emission of inorganic quantum dots.[9,10]

Nowadays, there are three main types of blue MREs reported in the literature, *i.e.*, boron–nitrogen,[8,10–12] carbonyl–nitrogen,[13–15] and indolocarbazole[16,17] based on scaffolds. Their FWHMs of the emission spectra range from 14 to 50 nm in solution states.[9,18] High-efficiency blue organic light-emitting diodes (OLEDs) with external quantum efficiencies (EQEs) of over 20% have been reported with these MREs.[9,18] Nonetheless, the device stabilities of MRE-based OLEDs are not sufficient[10,19] compared with those of conventional OLEDs with D–A type TADF emitters, since most MREs have a long triplet lifetime, *i.e.*, a slow reverse intersystem crossing (RISC) rate (k_{RISC}).[7,20–22] Thus, at present, MREs are found to be useful as the terminal emitter (TE) in hyperfluorescence OLEDs.[23–25] Indeed, having stable blue D–A type TADF emitters with narrow emissions provides a more straightforward solution. However, the reports on blue narrow-emission (FWHM ≤ 50 nm) D–A type emitters are limited. There are only a few reports on boron-containing narrow-emission D–A type TADF emitters in the literature (Table S1†).[18,26–29] As a result, it would be interesting to develop non-boron based narrow emissive D–A type TADF emitters.

[a]*Center for Organic Photonics and Electronics Research (OPERA), Kyushu University, Motooka, Nishi, Fukuoka 819-0395, Japan. E-mail: chinyiu.chan@opera.kyushu-u.ac.jp; adachi@cstf.kyushu-u.ac.jp*

[b]*International Institute for Carbon Neutral Energy Research (I2CNER), Kyushu University, 744 Motooka, Nishi, Fukuoka 819-0395, Japan*

† Electronic supplementary information (ESI) available. See https://doi.org/10.1039/d2sc02478k

‡ These authors contributed equally to this work.

This report explores a new class of blue D–A type TADF emitters with small FWHMs. Herein, a new acceptor core called carbazole-2-carbonitrile (CCN) is introduced. Three narrow-emission deep-blue DA-type TADF emitters based on CCN, namely **3CzCCN**, **3MeCzCCN**, and **3PhCzCCN**, have been synthesized and characterized. The three deep-blue TADF emitters display narrow charge-transfer (CT) emissions with FWHMs $\leq$ 50 nm in toluene and high photoluminescence quantum yields (PLQYs) of up to 85%. High-efficiency TADF OLEDs based on the three emitters have been fabricated, resulting in high maximum EQEs of up to 17.5% and deep-blue emissions with the *y*-coordinate < 0.2.

Results and discussion

Molecular design, synthesis, and DFT calculations

Benzonitrile is a promising candidate as a strong acceptor for constructing a stable blue D–A type TADF emitter; however, the resulting TADF emitters always show broad emission bands (60 to 100 nm) in the solution state, which is due to the formation of a strong CT state.[4] It is anticipated that the emission band of blue D–A type emitters can be narrowed by lowering the electron-accepting ability and increasing the steric hindrance of the acceptor core.[30] In this study, a new acceptor core, *i.e.* CCN, is introduced by fusing carbazole with the benzonitrile core. The high steric hindrance on the CCN acceptor core can effectively restrict the bond rotations of the donors, thus narrowing the emission band. The molecular design concept of blue CCN-based TADF emitters is shown in Scheme 1. In the synthetic route of **3CzCCN**, **3MeCzCCN**, and **3PhCzCCN**, a CCN acceptor was synthesized by the deprotonation of 2,3,5,6-tetrafluoro-5′-methyl-2′-(*p*-tolylamino)-[1,1′-biphenyl]-4-carbonitrile (**L1**) with the help of sodium hydride in *N*,*N*-dimethylformamide, followed by intramolecular aromatic nucleophilic substitution (Scheme 2). After that, various carbazole donor units were deprotonated by sodium hydride in *N*,*N*-dimethylformamide and reacted with the CCN unit at 150 °C. **3CzCCN**, **3MeCzCCN**, and **3PhCzCCN** were obtained with high yields. All final products were purified by temperature-gradient sublimation under vacuum after column chromatography to obtain highly pure materials, which were then used to fabricate OLEDs by vacuum deposition. All three TADF emitters have been characterized by ^{1}H NMR spectroscopy and atmospheric-pressure chemical ionization-electron ionization (APCI-EI) mass spectrometry (Fig. S1–S13†). Satisfactory elemental analyses have also been obtained.

To investigate the differences among the geometric and optical properties of **3CzCCN**, **3MeCzCCN**, and **3PhCzCCN**, quantum-chemical calculations were performed using time-dependent density functional theory (TD-DFT) at the B3LYP/6-31G(d) level. The calculated energy levels of the HOMO and LUMO, and the optimized geometries of **3CzCCN**, **3MeCzCCN**, and **3PhCzCCN**, are shown in Fig. 1. The typical dihedral angles between carbazole donor units and the benzonitrile unit in **4CzBN** and **5CzBN** are usually 60°;[20] however, the dihedral angles of **3CzCCN**, **3MeCzCCN**, and **3PhCzCCN** ranged from 75 to 87°, which further indicates the higher steric environment around the CCN acceptor core. The LUMOs of the three emitters are located on the CCN core. The HOMO of **3CzCCN** is located on the two carbazole units, while the HOMOs of **3MeCzCCN** and **3PhCzCCN** are only located on one carbazole derivative. The DFT-calculated ΔE_{ST} values of **3CzCCN**, **3MeCzCCN**, and **3PhCzCCN** are found to be 0.12, 0.10 and 0.07 eV, respectively. The oscillator strengths (*f*) calculated for the three compounds

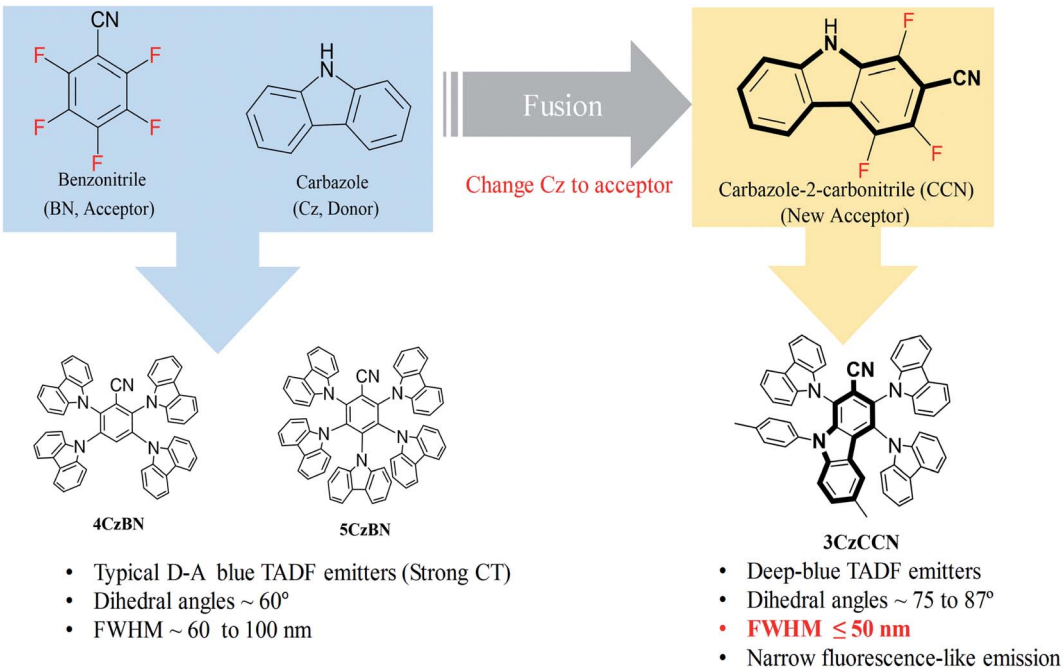

Scheme 1 New acceptor (CCN) by fusing carbazole and benzonitrile for narrow CT emissions of deep-blue D–A type TADF emitters.

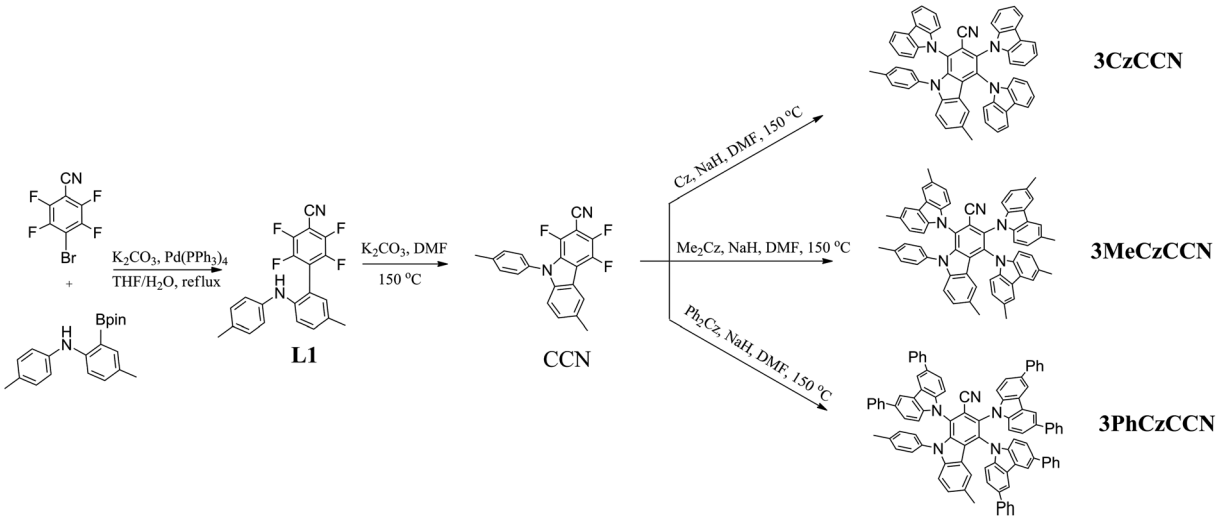

Scheme 2 Synthetic scheme of three CCN-based TADF emitters, **3CzCCN**, **3MeCzCCN**, and **3PhCzCCN**.

are found to be 0.0157, 0.0151, and 0.0177, respectively. The calculated *f* values are moderate; however, high PLQYs can still be expected when non-radiative decay is suppressed. Furthermore, it is known that a large difference in the electronic energies between a singlet energy state (S_1) and a ground state (S_0), *i.e.*, $\Delta E(E_{(S_1@S_0)} - E_{(S_1@S_1)})$, where $E_{(S_1@S_0)}$ is the electronic energy of S_1 at the optimized S_0 and $E_{(S1@S1)}$ is the electronic energy of S_1 at the optimized S_1 structure, and/or a large average change in the bond length between S_1 and S_0 will give rise to a larger FWHM in an emission spectrum.[10] The average change in the bond length and $\Delta E(E_{(S_1@S_0)} - E_{(S_1@S_1)})$ of **4CzBN** and **3CzCCN** have been calculated according to the literature (Tables S2 and S3†).[10] **4CzBN** shows a larger average change in the bond length and $\Delta E(E_{(S_1@S_0)} - E_{(S_1@S_1)})$ of 0.007884 Å and 328 meV, respectively, which gives rise to the broad emission band in toluene solution with an FWHM of 63 nm (375 meV).[7] On the other hand, **3CzCCN** shows smaller values of 0.006947 Å and 269 meV, respectively, which indicates the possibility of a smaller FWHM in the emission. The average change in the bond length and $\Delta E(E_{(S_1@S_0)} - E_{(S_1@S_1)})$ of **3MeCzCCN** and **3PhCzCCN** are also smaller than those of **4CzBN**, which are (0.006828 Å, 280 meV) and (0.004897 Å, 258 meV), respectively. On the other hand, **4CzBN** also shows a larger reorganization energy, *i.e.*, $\Delta E(E_{(S_1@S_0)} - E_{(S_1@S_1)}) + \Delta E(E_{(S_0@S_1)} - E_{(S_0@S_0)})$ of 719 meV, whereas **3CzCCN**, **3MeCzCCN** and **3PhCzCCN** show a smaller reorganization energy of 548, 574 and 523 meV, respectively. Additionally, when we compared the dihedral angles of the 4 C–N bonds of **4CzBN** and three CCN-based emitters at the S_0 ground state and S_1 excited state, it is found that the sum of changes in the dihedral angle in **4CzBN** (55.7°) is larger than that of **3CzCCN** (37.7°), **3MeCzCCN** (31.7°) and **3PhCzCCN** (20.4°), which further confirms their smaller distortion in the S_1 of the three emitters (Table S4†). On the other hand, the natural transition orbitals (NTOs) of the three emitters at singlet and triplet excited states are calculated (Table S5†). The singlet excited states of the three emitters are found to have a charge-transfer character. In the triplet excited states, since there are partial overlaps between holes and electrons on the CCN acceptor, the triplet excited states of the three emitters are found to be hybridized local and charge transfer (HLCT) in nature.

Photophysical, thermal, and electrochemical properties

The photophysical properties of the three emitters in toluene solutions have been first studied. In the UV-vis absorption spectra, the π–π transition band below 350 nm and the CT transition band at around 400 nm are found in all emitters.[31] Upon excitation at 340 nm, **3CzCCN**, **3MeCzCCN**, and **3PhCzCCN** display structure-less deep-blue emission at 439, 453, and 457 nm, respectively (Fig. 1b and Table 1). Emissions from the three emitters originated from the charge-transfer excited state which is confirmed by the solvatochromic study on emission (Fig. S14–S16†). Interestingly, all emitters show emissions with narrow FWHMs of less than 50 nm, which is unusual for D–A type blue TADF emitters. Meanwhile, the PLQYs of **3CzCCN**, **3MeCzCCN**, and **3PhCzCCN** are found to be 37, 59, and 85%, respectively, in degassed toluene solutions. The singlet energy levels of **3CzCCN**, **3MeCzCCN**, and **3PhCzCCN** are 3.02, 2.93, and 2.89 eV, respectively, while their corresponding triplet energy levels (T_1s) are 2.70 eV, 2.67, and 2.66. Such a small change in T_1s indicates that the triplet excited states are located on the acceptor CCN core. The calculated ΔE_{ST}s of **3CzCCN**, **3MeCzCCN**, and **3PhCzCCN** are found to be 0.32, 0.26, and 0.23 eV, respectively. On the other hand, the photophysical properties of doped films are also studied, in which 10 wt% of each emitter is doped in a host material, 3,3′-di(9*H*-carbazol-9-yl)-1,1′-biphenyl (mCBP). In the doped film, the emissions of **3CzCCN**, **3MeCzCCN**, and **3PhCzCCN** are found to be 451, 466, and 469 nm, respectively, which are slightly redshifted compared to those in toluene solutions. To estimate the accurate ΔE_{ST}s in doped films, the S_1s of 10 wt%-doped films of **3CzCCN**, **3MeCzCCN**, and **3PhCzCCN** are found to be 2.92, 2.86, and 2.84 eV, respectively, which are

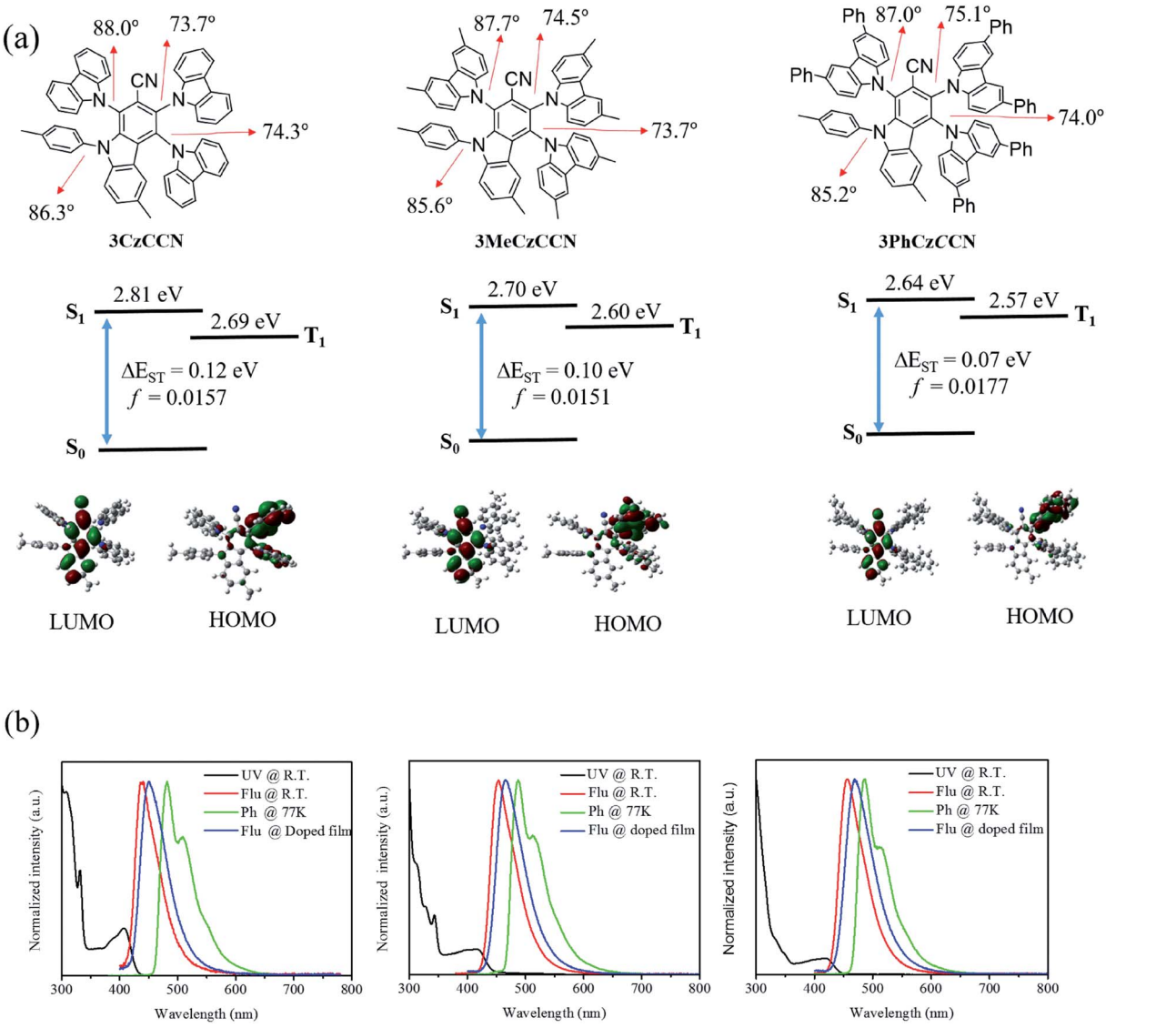

Fig. 1 (a) Molecular structures of **3CzCCN**, **3MeCzCCN**, and **3PhCzCCN** and their corresponding DFT calculations based on B3LYP/6-31G(d). (b) Photophysical properties of **3CzCCN**, **3MeCzCCN**, and **3PhCzCCN** in toluene solution (10^{-5} M) and doped in an mCBP host with 10 wt%.

calculated from the fluorescence spectrum at 77 K (Fig. S17†), while their corresponding T_1s are all found to be 2.63 eV, which are calculated from the phosphorescence spectrum at 77 K. The resulting ΔE_{ST}s in doped films are 0.29, 0.23, and 0.19 eV, respectively. On the other hand, the FWHMs of the emission spectra in doped films are slightly broadened. The temperature-dependent decay profiles of the three doped films are studied and depicted in Fig. 2, which clearly confirm the TADF

Table 1 Basic photophysical parameters of **3CzCCN**, **3MeCzCCN**, and **3PhCzCCN**

	In Toluene						10 wt% in mCBP										
Material	λ_{abs} (nm)	λ_{max} (nm)	FWHM (nm)	Φ_{Air}[a] (%)	Φ_{Ar}[b] (%)	ΔE_{ST} (eV)	λ_{max} (nm)	FWHM (nm)	Φ_{Ar} (%)	Φ_p[c] (%)	Φ_d[d] (%)	τ_p (ns)	τ_d (μs)	k_r (10^7 s^{-1})	k_{nr} (10^8 s^{-1})	k_{ISC} (10^8 s^{-1})	k_{RISC} (10^4 s^{-1})
3CzCCN	409	439	45	27	37	0.32	451	51	40	35	5	3.8	180	9.1	1.36	1.72	0.1
3MeCzCCN	417	453	48	21	59	0.26	466	54	61	44	17	5.1	47	8.6	0.55	1.1	1.5
3PhCzCCN	421	457	48	32	85	0.23	469	53	72	50	22	6.2	34	8.1	0.31	0.80	2.6
4CzBN[e]	403	441	63	9	63	0.23	460	89	51	14	37	3.3	14	4.4	0.42	2.59	21.5

[a] PLQY in aerated toluene. [b] PLQY in degassed toluene. [c] Prompt intensity. [d] Delayed intensity. [e] Ref. 7.

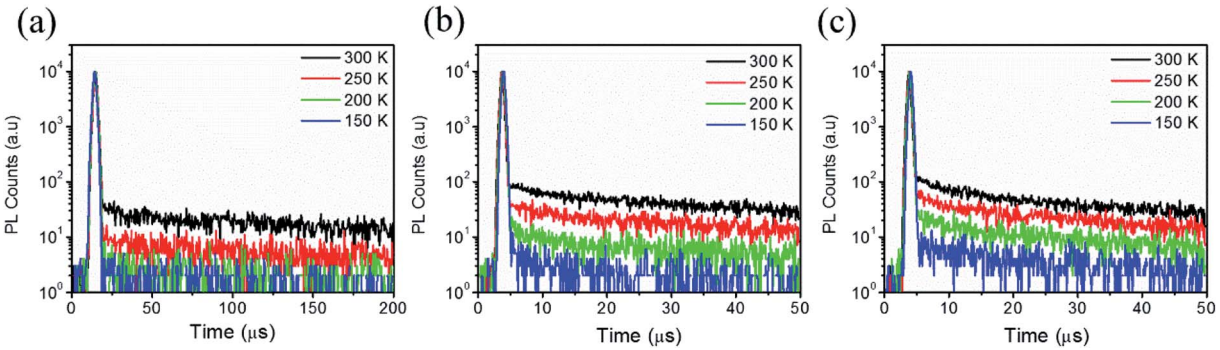

Fig. 2 Temperature dependent decay profiles of (a) **3CzCCN**, (b) **3MeCzCCN**, and (c) **3PhCzCCN** in an mCBP host with 10 wt%.

properties of the three emitters. The large ΔE_{ST} of **3CzCCN** results in a long-delayed lifetime (τ_d) of 180 μs. With the narrower ΔE_{ST}s of **3MeCzCCN** and **3PhCzCCN**, they show shorter τ_ds of 47 and 34 μs, respectively. The k_{RISC} of **3PhCzCCN** is calculated to be 2.6×10^4 s^{-1},[7] which is the highest amongst that of the three emitters (Table 1). The relatively slow τ_ds are mainly due to the large ΔE_{ST}s. It is expected that the k_{RISC} of CCN-based TADF emitters can be further enhanced with a rational molecular design of molecules that possess small ΔE_{ST}s in the future. The electrochemical properties of **3CzCCN**, **3MeCzCCN**, and **3PhCzCCN** are determined by cyclic voltammetry in *N*,*N*-dimethylformamide solutions (Fig. S18–S20, Table S6†). The potentials for an oxidative scan of **3CzCCN**, **3MeCzCCN**, and **3PhCzCCN** are +1.00, +0.87 and +0.84 V *vs.* Fc/Fc^+, respectively, which resulted in the corresponding HOMO values of −5.80, −5.67, and −5.64 eV, respectively. On the other hand, the potentials for a reductive scan of **3CzCCN**, **3MeCzCCN**, and **3PhCzCCN** are −2.14, −2.18, and −2.11 V *vs.* Fc/Fc^+, respectively, which resulted in the corresponding LUMO values of −2.66, −2.62, and −2.69 eV, respectively. The thermogravimetry-differential thermal analysis (TG-DTA) is performed to examine the thermal stabilities of the three CCN-based TADF emitters. From TG-DTA measurement, it is found that **3CzCCN**, **3MeCzCCN**, and **3PhCzCCN** show excellent thermal stabilities with T_ds (5% weight loss) of 433, 434, and 555 °C, respectively (Fig. S21 and Table S7†).

OLED performance

The following configuration: indium-tin-oxide (ITO)-coated glass (100 nm)/HAT-CN (10 nm)/TrisPCz (30 nm)/mCBP (5 nm)/mCBP: 10 wt% of **3CzCCN** (device A) or **3MeCzCCN** (device B) or **3PhCzCCN** (device C) (30 nm)/SF3-TRZ (10 nm)/SF3-TRZ: 30 wt% Liq (20 nm)/Liq (2 nm)/Al (100 nm) is used to confirm OLED characteristics. 1,4,5,8,9,11-hexaazatriphenylenehexacarbonitrile (HAT-CN) is the hole-injection layer, 9-phenyl-3,6-bis(9-phenyl-9*H*-carbazol-3-yl)-9*H*-carbazole (TrisPCz) is the hole-transporting layer, mCBP is used for exciton-blocking and host layers, 2-(9,9′-spirobi[fluoren]-3-yl)-4,6-diphenyl-1,3,5-triazine (SF3-TRZ) is the electron-transporting layer, and 8-hydroxyquinolinolato-lithium (Liq) and Al are the electron injection and cathode layers, respectively (Fig. 3 and S22†). All the device characteristics are shown in Fig. 3, S23–S26,† and Table 2. The devices A–C are fabricated based on an emitting layer (EML) consisting of 10 wt% of the corresponding emitters doped in an mCBP host. All devices display deep-blue EL peaks with λ_{max}s of 445, 462, and 462 nm, respectively. The FWHMs of devices A–C are found to be 52, 59, and 55 nm, respectively, which are slightly broader than those in toluene solutions. The slightly larger values of FWHMs in ELs may be due to the electronic interactions, *i.e.*, polarization effects, between hosts and emitters. When the emitters are doped in a polar host (2,8-bis(diphenyl-phosphoryl)-dibenzo[*b*,*d*]thiophene, PPT), it is found that the emission peaks are redshifted and broadened

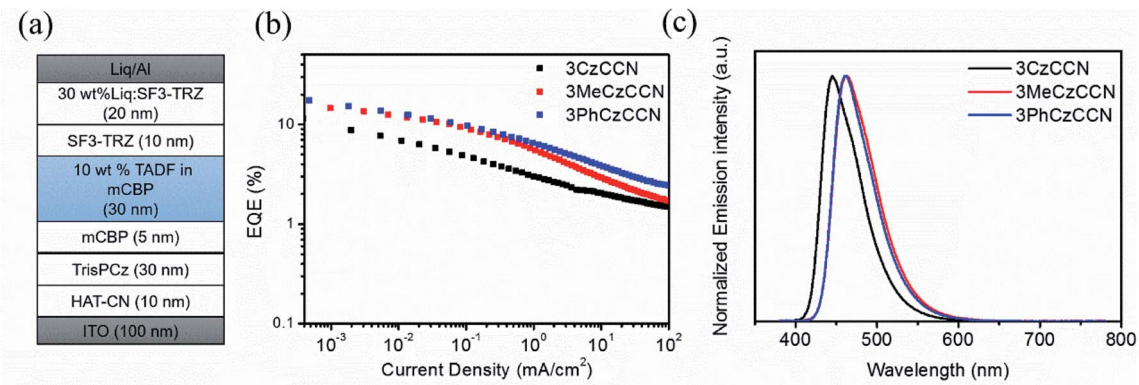

Fig. 3 OLED performance of devices A–C. (a) TADF OLED structure; (b) EQE *versus* current density; (c) EL spectra of devices A–C at 5 V.

Table 2 Device performance of deep-blue TADF OLEDs

Device	Dopant	V_{on}[a] (V)	L_{max}[b] (cd m^{-2})	EQE[c] (%)	λ_{EL}[d] (nm)	FWHM (nm)	CIE (x, y)[d]
A	**3CzCCN**	3.8	1358	11.5/3.9/2.2	445	52	0.15, 0.09
B	**3MeCzCCN**	3.6	2023	15.8/9.4/4.8	462	59	0.14, 0.17
C	**3PhCzCCN**	3.8	6451	17.5/10.6/6.3	462	55	0.14, 0.15

[a] Voltage at 1 cd m^{-2}. [b] At maximum. [c] External quantum efficiency: values at maximum, at 10 cd m^{-2}, and at 100 cd m^{-2}. [d] Value at 5 V.

(Fig. S27†). Nevertheless, the small FWHMs in ELs of CCN-based devices are one of the smallest values amongst the values reported in D–A type blue TADF OLEDs.[18] Doping **3CzCCN** in an mCBP host results in a decent PLQY of 40%, which limits the maximum external quantum efficiency (EQE_{max}) of device A to 11.5%. With an increase in PLQY of the **3MeCzCCN** and **3PhCzCCN** doped films, devices B and C show higher EQE_{max}s of 15.8% and 17.5%, respectively. The $CIE_{x,y}$s of devices A–C are found to be (0.15, 0.09), (0.14, 0.17), and (0.14, 0.15), respectively, which all display deep-blue emission. Compared to a **4CzBN**-based device, CCN-based devices showed severe rolloff issues, which may be due to the longer decay lifetimes and imbalanced carrier transport properties (Fig. S26†). It is expected that increasing the dopant concentration may help to balance the carrier transport properties.[32] Thus, the effect of the dopant concentration on the EQE is studied with **3PhCzCCN** (Fig. S28†). By increasing the dopant concentration to 20 wt% or 30%, the rolloff issue becomes less severe; however, at a doping concentration of 30 wt%, the maximum EQE drops to 15.6%, which may be due to the effect of concentration quenching. The device lifetimes of devices A and B are too short to be measured, while device C shows the best LT50 of 10 h and 65 h at an initial luminance of 500 and 100 cd m^{-2}, respectively (Fig. S29†). When the dopant concentration of **3PhCzCCN** is increased from 10 to 30 wt%, a LT50 of over 50 h is achieved at an initial luminance of 500 cd m^{-2} (Fig. S30†), which is comparable to that of **4CzBN**-devices.[20] The relatively fair device lifetime might be originated from the long-delayed lifetime of **3PhCzCCN**. It is believed that the delayed lifetime of CCN-based TADF emitters can be shortened *via* rational molecular design, thus enhancing the device stability in the future. It is also believed that the device stability can be further improved with the help of device engineering, *e.g.*, other host materials.

Conclusion

A series of deep-blue D–A type TADF emitters based on a new acceptor core, CCN, has been successfully synthesized. The newly synthesized CCN-based TADF emitters display narrow CT emission in toluene with FWHMs < 50 nm, which are one of the smallest values of FWHMs reported in D–A type blue TADF emitters. The unexpected narrow emissions of CCN-based TADF emitters originated from the steric hindrance environment on the CCN acceptor, which causes less structural distortion in the excited state compared to the ground state. The hypothesis is further supported by the DFT calculations, in which all CCN emitters show smaller reorganization energies than that of the conventional **4CzBN**. Furthermore, it was also found that the sum of the changes in dihedral angles of C–N bonds in CCN-based emitters is smaller in the excited states, which is consistent with the small reorganization energy.

Although their FWHMs are not as narrow as those of blue MREs, they are comparable to or even narrower than some of the conventional blue fluorescence emitters. OLEDs based on this series of CCN-based TADF emitters have resulted in high maximum EQEs of up to 17.5%. The CCN-based deep-blue TADF emitters in this work definitely enrich the molecular library of narrow-emission blue D–A type TADF emitters, which are seldom reported in the literature.

Experimental section

All reagents were used as received from commercial sources and were used without further purification. 9*H*-Carbazole was purchased from Ushio Chemix Co. with a purity of 99.9% (without isomer), and 3,6-dimethyl-9*H*-carbazole and 3,6-diphenyl-9*H*-carbazole were purchased from Suzhou Ge'ao New Material Co., Ltd. with a purity of 99.7% and 98.0%, respectively. Chromatographic separations were carried out using silica gel (200–300 nm). The three materials investigated in this study were synthesized by following the procedures described below. All compounds were purified twice by temperature gradient vacuum sublimation. ^{1}H nuclear magnetic resonance (NMR) spectra were obtained in $CDCl_3$ with a Bruker Biospin Avance-III 500 NMR spectrometer at ambient temperature. Chemical shifts (δ) are given in parts per million (ppm) relative to tetramethylsilane (TMS; $\delta = 0$) as the internal reference. Mass spectra were measured in positive-ion atmospheric-pressure chemical ionization (APCI) mode on a Waters 3100 mass detector. Elemental analyses (C, H, and N) were carried out with a Yanaco MT-5 elemental analyzer. Toluene solutions containing these three materials (0.1 mM) were prepared to investigate their absorption and photoluminescence characteristics in the solution state. Thin-film samples (10 wt%-**3CzCCN**, **3MeCzCCN**, and **3PhCzCCN** doped in an mCBP host with a thickness of 100 nm) were deposited on quartz glass substrates by vacuum evaporation to study their exciton confinement properties in the film state. Ultraviolet-visible absorption (UV-vis) and photoluminescence (PL) spectra were recorded on a PerkinElmer Lambda 950 KPA spectrophotometer and a JASCO FP-8600 spectrofluorometer. Absolute PL quantum yields were measured on a Quantaurus-QY measurement system (C11347-11, Hamamatsu Photonics) under a nitrogen flow and all samples were excited at 340 nm. The prompt and delayed PL spectra of the samples were measured under vacuum using

a streak camera system (Hamamatsu Photonics, C4334) equipped with a cryostat (Iwatani, GASESCRT-006-2000, Japan). Cyclic voltammetry (CV) was carried out on a CHI600 voltammetric analyzer at room temperature with a conventional three-electrode configuration consisting of a platinum disk working electrode, a platinum wire auxiliary electrode and an Ag wire pseudo-reference electrode with ferrocenium–ferrocene (Fc^+/Fc) as the internal standard. Argon-purged *N*,*N*-dimethylformamide was used as a solvent for scanning the oxidation with tetrabutylammonium hexafluorophosphate ($TBAPF_6$) (0.1 M) as the supporting electrolyte. The cyclic voltammograms were obtained at a scan rate of 100 mV s^{-1}. Thermal gravimetry-differential thermal analysis (TG-DTA) was performed using a Bruker TG-DTA 2400SA with a heating rate of 10 °C min^{-1} under a nitrogen atmosphere.

Quantum chemical calculations

All calculations were carried out using the Gaussian 16 program package. The geometries in the ground state were optimized *via* DFT calculations at the B3LYP/6-31G* level. TD-DFT calculations for the $S_0 \rightarrow S_1$ and $S_0 \rightarrow T_1$ transitions using the B3LYP functional were then performed according to the optimized geometries of the lowest-lying singlet and triplet states, respectively.

Device fabrication and measurements

The OLEDs were fabricated through vacuum deposition of the materials at *ca.* 10^{-5} Pa onto indium-tin-oxide-coated glass substrates having a sheet resistance of *ca.* 15 Ω $\square^{-1}$. The indium-tin oxide surface was cleaned ultrasonically and sequentially with acetone, isopropanol, and deionized water, then dried in an oven, and finally exposed to ultraviolet light and ozone for about 10 min. Organic layers were deposited at a rate of 1–2 Å s^{-1}. Subsequently, Liq was deposited at 0.1–0.2 Å s^{-1}. The devices were exposed once to nitrogen gas after the formation of the organic layers to allow the fixing of a metal mask to define the cathode area. For all OLEDs, the emitting areas were determined by the overlap of two electrodes to be 0.04 cm^2. The *J*–*V*-luminance characteristics were evaluated using a Keithley 2400 source meter and an absolute external quantum efficiency (EQE) measurement system (C9920-12, Hamamatsu Photonics, Japan). Device operational stability was measured using a luminance meter (CS-2000, Konica Minolta, Japan) at a constant DC current at room temperature.

Data availability

The data that support the plots within the paper are available from the corresponding author upon reasonable request.

Author contributions

C. A. supervised the project. C.-Y. C. conceived the idea and designed, synthesized, and characterized the blue TADF emitters. C.-Y. C. and Y.-T. L. fabricated the OLEDs and characterized the devices. M. M. performed the theoretical calculations. C.-Y. C., M. M., and C. A. contributed to the manuscript writing. Y.-T. L., M. M., K. G., Y. T., and H. N. provided suggestions on the experiments and writing the manuscript. All authors discussed the progress of the research and reviewed the manuscript.

Conflicts of interest

The authors declare no competing interests.

Acknowledgements

The authors acknowledge Ms N. Nakamura and Ms K. Kusuhara for their technical assistance with this research. This work was supported financially by the JSPS Core-to-Core Program (grant number: JPJSCCA20180005) and Kyulux Inc.

References

1 J.-J. Zhu, Y. Chen, Y.-H. Xiao, X. Lian, G.-X. Yang, S.-S. Tang, D. Ma, Y. Wang and Q.-X. Tong, *J. Mater. Chem. C*, 2020, **8**, 2975.
2 C.-Y. Chan, Y.-C. Wong, M.-Y. Chan, S.-H. Cheung, S.-K. So and V. W.-W. Yam, *ACS Appl. Mater. Interfaces*, 2016, **8**, 24782.
3 J.-S. Huh, Y. H. Ha, S.-K. Kwon, Y.-H. Kim and J.-J. Kim, *ACS Appl. Mater. Interfaces*, 2020, **12**, 15422.
4 H. Uoyama, K. Goushi, K. Shizu, H. Nomura and C. Adachi, *Nature*, 2012, **492**, 234.
5 M. Y. Wong and E. Zysmon-Colman, *Adv. Mater.*, 2017, **29**, 1605444.
6 C.-Y. Chan, L.-S. Cui, J. U. Kim, H. Nakanotani and C. Adachi, *Adv. Funct. Mater.*, 2018, **28**, 1706023.
7 C.-Y. Chan, M. Tanaka, H. Nakanotani and C. Adachi, *Nat. Commun.*, 2018, **9**, 5036.
8 T. Hatakeyama, K. Shiren, K. Nakajima, S. Nomura, S. Nakatsuka, K. Kinoshita, J. Ni, Y. Ono and T. Ikuta, *Adv. Mater.*, 2016, **28**, 2777.
9 S. M. Suresh, D. Hall, D. Beljonne, Y. Olivier and E. Zysmon-Colman, *Adv. Funct. Mater.*, 2020, **30**, 1908677.
10 Y. Kondo, K. Yoshiura, S. Kitera, H. Nishi, S. Oda, H. Gotoh, Y. Sasada, M. Yanai and T. Hatakeyama, *Nat. Photonics*, 2019, **13**, 678.
11 M. Yang, I. S. Park and T. Yasuda, *J. Am. Chem. Soc.*, 2020, **142**, 19468.
12 Y. Zhang, D. Zhang, T. Huang, A. J. Gillet, Y. Liu, D. Hu, L. Cui, Z. Bin, G. Li, J. Wei and L. Duan, *Angew. Chem., Int. Ed.*, 2021, **60**, 20498.
13 D. Sun, S. M. Suresh, D. Hall, M. Zhang, X. Si, D. B. Cordes, A. M. Z. Slawin, Y. Olivier, X. Zhang and E. Zysmon-Colman, *Mater. Chem. Front.*, 2020, **4**, 2018.
14 X. Li, Y.-Z. Shi, K. Wang, M. Zhang, C.-J. Zheng, D.-M. Sun, G.-L. Dai, X.-C. Fan, D.-Q. Wang, W. Liu, Y.-Q. Li, J. Yu, X.-M. Qu, C. Adachi and X.-H. Zhang, *ACS Appl. Mater. Interfaces*, 2019, **11**, 13472.
15 Y. Yuan, X. Tang, X.-Y. Du, Y. Hu, Y.-J. Yu, Z. Q. Jiang, L.-S. Liao and S.-T. Lee, *Adv. Opt. Mater.*, 2019, **7**, 1801536.

16 D. Hall, K. Stavrou, E. Duda, A. Danos, S. Bagnich, S. Warriner, A. M. Z. Slawin, D. Beljonne, A. Kohler, A. Monkman, Y. Olivier and E. Zysmon-Colman, *Mater. Horiz.*, 2022, **9**, 1068.
17 J. Wei, C. Zhang, D. Zhang, Y. Zhang, Z. Liu, Z. Li, G. Yu and L. Duan, *Angew. Chem., Int. Ed.*, 2021, **60**, 12269.
18 J.-M. Teng, Y.-F. Wang and C.-F. Chen, *J. Mater. Chem. C*, 2020, **8**, 11340.
19 H. Tanaka, S. Oda, G. Ricci, H. Gotoh, K. Tabata, R. Kawasumi, D. Beljonne, Y. Olivier and T. Hatakeyama, *Angew. Chem., Int. Ed.*, 2021, **60**, 17910.
20 D. Zhang, M. Cai, Y. Zhang, D. Zhang and L. Duan, *Mater. Horiz.*, 2016, **3**, 145.
21 X. Liu, C.-Y. Chan, F. Mathevet, M. Mamada, Y. Tsuchiya, Y.-T. Lee, H. Nakanotani, S. Kobayashi, M. Shiochi and C. Adachi, *Small Science*, 2021, **1**, 200057.
22 H. Noda, H. Nakanotani and C. Adachi, *Sci. Adv.*, 2018, **4**, eaao6910.
23 C.-Y. Chan, M. Tanaka, Y.-T. Lee, Y.-W. Wong, H. Nakanotani and C. Adachi, *Nat. Photonics*, 2021, **15**, 203.
24 S. O. Jeon, K. H. Lee, J. S. Kim, S.-G. Ihn, Y. S. Chung, J. W. Kim, H. Lee, S. Kim, H. Choi and J. Y. Lee, *Nat. Photonics*, 2021, **15**, 208.
25 K. W. Lo, G. S. M. Tong, G. Cheng, K.-H. Low and C.-M. Che, *Angew. Chem., Int. Ed.*, 2022, **61**, e202115515.
26 A. Khan, X. Tang, X. Zhong, Q. Wang, S.-Y. Yang, F.-C. Kong, S. Yuan, A. Sandanayaka, C. Adachi, Z.-Q. Jiang and L.-S. Liao, *Adv. Funct. Mater.*, 2021, **31**, 2009488.
27 G. Xia, C. Qu, Y. Zhu, J. Ye, K. Ye, Z. Zhang and Y. Wang, *Angew. Chem., Int. Ed.*, 2021, **60**, 9598.
28 D. H. Ahn, S. W. Kim, H. Lee, I. J. Ko, D. Karthik, J. Y. Lee and J. H. Kwon, *Nat. Photonics*, 2019, **13**, 540.
29 J. Han, Z. Huang, J. Miao, Y. Qiu, Z. Xie and C. Yang, *Chem. Sci.*, 2022, **13**, 3402.
30 Y. J. Cho, S. K. Jeon, S.-S. Lee, E. Yu and J. Y. Lee, *Chem. Mater.*, 2016, **28**, 5400.
31 T. Hosokai, H. Matsuzaki, H. Nakanotani, K. Tokumaru, T. Tsutsui, A. Furube, K. Nasu, H. Nomura, M. Yahiro and C. Adachi, *Sci. Adv.*, 2017, **3**, e1603282.
32 H. Nakanotani, K. Masui, J. Nishide, T. Shibata and C. Adachi, *Sci. Rep.*, 2013, **3**, 2127.